Materials Research. 2025; 28:e20240468
DOI: https://doi.org/10.1590/1980-5373-MR-2024-0468

Development of Empirical Relationships for Prediction of Wear Properties of AA6092/B_4C Aluminum Matrix Composites Produced Using Friction Stir Welding

Umar Mohamed Jamaludeen*[a]

[a]*Annamalai Polytechnic College, Department of Mechanical Engineering, Chettinad, Tamil Nadu, India.*

Received: October 17, 2024; Revised: December 04, 2024; Accepted: January 19, 2025

Aluminum Metal matrix composites (AMMCs) have gained significant attention in the automotive and aerospace industries due to their outstanding mechanical properties, combined with their lightweight and fuel-efficient characteristics. AMMCs have also garnered significant attention from researchers due to their potential to minimize the wear of counter face materials. This study investigates the dry sliding wear behavior of aluminum-based hybrid MMCs using an experimental approach. Friction Stir Welding (FSW) has emerged as a promising solid-state technique for welding AMMCs. The FSW experiments were designed using a Central Composite Rotatable Design (CCRD) with four factors and five levels. Empirical models were developed to predict the influence of FSW process parameters including tool rotational speed (TRS), Welding Speed (WS), Axial Load (AL), and the percentage of Boron Carbide (B_4C) reinforcement on key properties such as wear rate and wear resistance of the AMMCs. The developed regression model was developed to minimize the wear rate using response surface methodology (RSM) method and predicted wear rate is found to be 154.21 x 10^{-5} mm^3/m. The maximum percentage errors for predicting optimal Wear Rate, and Wear Resistance (WR) were + 5.39%, and + 2.65%, respectively. The wear resistance of the AMMCs was also improved by following Friction Stir Welding (FSW).

Keywords: *Friction Stir Welding, Aluminium alloy AA6092, Boron Carbide, Wear rate, Wear resistance.*

1. Introduction

Aluminum Metal matrix composites (AMMCs) exhibit a range of remarkable mechanical properties, such as high stiffness, excellent wear resistance at elevated temperatures, high specific strength and low thermal expansion[1,2]. One of the most promising applications for these composites is in wear-resistant materials. AMMCs have emerged as viable alternatives to conventional monolithic aluminum alloys in various industrial applications like aerospace, automotive, defence, naval, electronics packaging, thermal management, and sports. Typically, the matrix consists of a lightweight metal reinforced with fibres, whiskers, or particles[3]. Among these, particle-reinforced composites are more cost-effective than other types. Their superior resistance to wear and abrasion is attributed to the hard particles embedded within the matrix. However, despite these advantageous characteristics, particle-reinforced AMMCs do have some drawbacks[4]. Notably, the inclusion of particles can make the material more brittle, reducing its ductility and negatively impacting machinability. AMMCs reinforced with materials such as SiC, TiB_2, Al_2O_3, TiC, and graphite have garnered significant research interest[5]. Among these reinforcements, B_4C has emerged as a particularly promising reinforcement particle for AMMCs due to its remarkable wear resistance, thermal and chemical stability, low density, and high hardness. This extremely hard boron-carbon ceramic, often referred to as black diamond, ranks as the third hardest synthetic material, following diamond and cubic boron nitride[6]. Additionally, it possesses good neutron absorption capabilities and allows for easy net shape workability. There is limited published research on the sliding wear behavior of AMMCs reinforced with B_4C. Dinaharan et al.[7] attempted to friction stir weld AA6061 with 0-10 wt.% ZrB_2 in-situ composites and developed empirical models to predict the sliding wear behavior of butt joints. It is reported that the joints fabricated with a TRS of 1150 rpm, a WS of 50 mm/min, and an AL of 6 kN exhibited the highest wear resistance.

Dinaharan et al.[8] investigated the effect of Friction Stir Welding (FSW) on the microstructure, mechanical, and wear properties of AA6061/ZrB_2 composites. Their findings showed that the weld zone exhibited higher hardness compared to the parent composite. The tensile strength of the welded joints was comparable to that of the parent composite. Additionally, the wear resistance of the composites improved after FSW. Hassan et al.[9] investigated the effects of Friction Stir Welding (FSW) processing parameters specifically tool geometry, rotational speed, and welding speed—on the wear characteristics of the welded joints in a hybrid aluminum matrix composite under dry sliding conditions. The study revealed that joints welded with a square pin profile exhibited superior wear resistance compared to other pin profiles. The findings highlighted that FSW processing parameters significantly influence the wear resistance of the welded joints, primarily due to various microstructural changes during welding that enhance the hardness and wear properties of the welded

*e-mail: umarmjamaludeen@gmail.com

zone. Kalaiselvan and Murugan[10] investigated the dry sliding wear behavior of a Friction Stir Welded aluminum (6061)-B_4C composite. It is reported that the optimal wear rate of 187.7003×10^{-5} mm^3/m was achieved under the following conditions: a TRS of 968 rpm, a WS of 1.29 mm/s, an AL of 9.94 kN, and a reinforcement content of 12 Wt.% B_4C.

Krishnamurthy et al.[11] investigated the impact of titanium diboride (TiB_2) loading on the dry sliding wear characteristics of aluminum 6063 matrix alloy-titanium diboride (Al/TiB_2) composite materials. The findings indicated that the composite reinforced with 10 wt.% TiB_2 exhibited superior wear resistance and a lower wear rate, making it a harder and stronger material compared to both the unreinforced matrix and the 5 wt.% TiB_2 reinforced Al-6063 composite. Khare et al.[12] studied the influence of process parameters on dry sliding wear behaviour of AA7075 composites (fabricated by reinforced with varying weight percentage of Al_2O_3 (8,10 and 12 wt.%) particles and weight percentages of B_4C (2, 3 and 4 wt. %)). It is also confirmed that by adding B_4C the wear of alumina reinforced composites has significantly reduced.

Hillary et al.[13] examined the dry sliding wear characteristics of a newly developed hybrid metal matrix composite made of Al6061 with 5% SiC and varying amounts of TiB_2 (2%, 4%, 6%, 8%, and 10 wt.%) fabricated via the stir casting method. The wear rate and coefficient of friction were measured using a pin-on-disc tribometer under various dry sliding conditions. The experimental results revealed that the addition of secondary hard ceramic TiB_2 particles significantly enhanced the wear behavior of the hybrid composite due to the formation of a Mechanically Mixed Layer (Fe_2O_3 layer). Suresh et al.[14] examined the tribological behavior of aluminum alloy (AA5083)/nano-Al_2O_3 metal matrix composites with varying reinforcement percentages of 2%, 4%, 6%, and 8% nano-Al_2O_3 particles. The study found that the hardness and wear resistance of the composites was superior to that of the unreinforced alloy, peaking at a 6% reinforcement level. Additionally, wear decreased with increasing reinforcement up to 6%, but further increases in particle content led to a deterioration in wear resistance due to changes in hardness.

Vijayakumar et al.[15] investigated the dry sliding wear rate of friction stir welded AA6262/AA5456 composites using the Taguchi method. Wear experiment was conducted by selecting appropriate process parameters, including load (LD), sliding speed (SS), and sliding distance (SE), to analyse the individual and combined effects of these parameters. The results indicated that the maximum wear rate was 0.01215 mm^3/Nm at a load of 50 N, a sliding distance of 600 m, and a sliding speed of 4 m/s. In contrast, the minimum wear rate of 0.00414 mm^3/Nm occurred at a different set of parameters: a load of 30 N, a sliding distance of 400 m, and a sliding speed of 6 m/s. Ship bulkheads are critical structural components that divide a ship into compartments, ensuring its structural integrity and safety. They are subjected to various stresses, including impact, vibration, and corrosion, which can significantly impact their lifespan. The incorporation of B_4C particles into an AA6092 aluminum matrix offers a novel approach to enhance the performance of ship bulkheads (watertight, fire-resistant and sound- insulating). The key advantages like increased hardness and strength, improve wear resistance, protective oxide layer, reduced weight. By utilizing B_4C-reinforced AA6092 alloy, ship builders can create lighter, stronger, and more durable bulkheads that meet the stringent requirements of the marine industry. This novel approach offers significant advantages in terms of safety, efficiency, and long-term performance. This study aims to develop empirical models to predict the sliding wear behavior of friction stir welded AA6092/ 0-10 wt.% of B_4C butt joints and to analyse the effect of process parameters on the wear rate and wear resistance of the welded joints. AA6092 was used as the matrix material. Experiments were conducted following the Central Composite Rotatable Design (CCRD). Several researchers have employed CCRD to design experiments and successfully developed precise empirical relationships to predict the influence of process parameters on various responses.

2. Scheme of Evaluation

2.1. Fabrication of AA6092/ B4C composite

The stir casting technique was used to fabricate AA6092/B_4C composites. A specially designed electric stir casting furnace with a bottom-pouring system was employed for this process. Cleaned AA6092 extruded rods, 25 mm in diameter, were placed into a coated stainless-steel crucible, and the furnace temperature was set to 1000°C. The chemical composition of AA6092 alloy is shown in Table 1. A coated stainless-steel stirrer, powered by an electric motor, was used to stir at the speed of 550 rpm to melt and ensure uniform incorporation of the B_4C reinforcement within the molten AA6092 alloy. Both the crucible and stirrer were coated with ceramic, refractory metal or graphite to avoid contamination at high temperatures. Preheated B_4C particles (3–4 μm in size) were added to the melt at the vortex's edge. To enhance the wettability of B_4C with the AA6092 matrix, magnesium, amounting to 2 wt.% of the total composite weight, was added. The B_4C particles were incorporated into the melt for 260 seconds, followed by further stirring for 1200 seconds before being poured into a preheated permanent mold (100 mm × 50 mm × 50 mm) using the bottom-pouring system. Argon gas was supplied at a constant flow rate of 2 lpm when the furnace temperature reached 650°C and continued until the molten composite was poured into the mold. AA6092/B_4C composites containing 0–10 wt.% of B_4C were produced in this way. 100 mm × 50 mm × 6 mm (Figure 1) were cut from the composite block using a wire-cut EDM process for FSW trials, process parameter optimization, and experiments based on the design matrix[16-18]. Additionally, the weight percentage of B_4C particles (W) was considered to assess its impact on Wear rate and Wear resistance.

Table 1. The chemical composition of AA6092 alloy matrix.

Element	Mg	Si	Fe	Mn	Cu	Cr	Zn	Ti	Al
Wt. %	1.2	0.4	0.3	0.15	0.7	0.15	0.25	0.15	Balance

Specimens measuring 100 mm × 50 mm × 6 mm were cut from each welded plate for testing. The dry sliding wear behavior was evaluated using a pin-on-disc wear apparatus (DUCOM TR20-LE) at room temperature, following the ASTM G99-04 standard. The polished surface of the pin was slid against a hardened chromium steel disc. The test was conducted with a sliding velocity of 1.5 m/s, a normal force of 25 N, and a sliding distance of 2500 m. These wear parameters were selected to achieve a steady-state wear based on preliminary trials[19]. A computer-aided data acquisition system monitored the height loss during the test. The volumetric loss was calculated by multiplying the cross-sectional area of the pin by the height loss. The Wear Rate (W) and Wear Resistance (R) were then calculated and are tabulated in Table 2[20].

$$W = V_l / SD \quad (1)$$

where W is Wear Rate in mm^3/m, V_l is Volumetric loss in mm^3 and SD is Sliding distance in mm

Figure 1. The fabricated stir cast AA6092/ B_4C composite plate.

$$R = (1 / W) \quad (2)$$

where R is Wear Resistance in (m/mm^3) and Where W is Wear Rate in mm^3/m

The relative wear rate is the ratio between wear rate of welded composite and wear rate of parent composite. It was computed as given below and also presented in Table 2.

$$R_w = W_w / W_p \quad (3)$$

where R_w is Relative wear rate, W_w is Wear rate of welded composite and W_p is Wear rate of parent composite

2.2. Identification of FSW process parameters

Based on preliminary trials and a review of the literature, several independent Friction Stir Welding (FSW) process parameters were identified as influencing Wear rate and Wear resistance. These parameters include tool pin profile (P), tool rotational speed (TRS), welding speed (WS), and axial load (AL). The key FSW parameters affecting joint properties are tool rotational speed, welding speed, and axial load, with the tool pin profile also playing a significant role in determining joint characteristics. A tool made of High Carbon High Chromium (HCHCr) steel, oil-hardened to 62 HRC, with a square pin profile, was used in this study. The tool dimensions—18 mm shoulder diameter, 5.7 mm pin length, 6 mm pin diameter, and 45 mm collet length[6,8,9,11] are shown in Figure 2. The chemical composition of HCHCr steel is detailed in Table 3. These square pin profiles were fabricated using Computerized Numerically Controlled (CNC) turning centres and Electrical Discharge Machines (EDM).

2.3. Identification of limits of FSW process parameters

The FSW window for achieving sound welds in aluminum metal matrix composites (AMMCs) is narrower than in unreinforced alloys due to the presence of ceramic particles trial welds were performed to establish the working ranges for all selected process parameters. Each trial weld was visually inspected for a smooth bead appearance and cross-sectioned to check for defects such as pinholes, tunnels, and wormholes in the weld zone. The process parameter limits were set based on achieving defect-free welds. For ease of recording and processing experimental data, the upper limit of each parameter was coded as +2, and the lower limit was coded as –2. The coded values for

Table 2. Wear Rate and Wear Resistance of AA6092 composites.

Sample No		1	2	3	4	5
% of compositions	AA6092	100	95	90	85	80
	B_4C	0	2.5	5	7.5	10
Wear Rate (1 x 10^{-5}) mm^3/m)		538	482	463	432	445
Wear Resistance (m/mm^3)		186	207	216	231	225

intermediate levels were calculated using the following Equation 4[17-20].

$$A_i = 2\left[2A - \left(A_{max} + A_{min}\right)\right] / \left(A_{max} - A_{min}\right) \quad (4)$$

where A_i is the essential coded value of a variable A; A is any value of the variable between A_{max} and A_{min}; A_{max} is the upper limit of the variable; A_{min} is the lower limit of the variable. The selected levels of the process parameters with their notations and units are depicted in Table 4.

2.4. Evolving an experimental design matrix

The experimental design matrix, presented in Table 4, follows a central composite rotatable full factorial design, consisting of 31 sets of coded conditions. The first 16 experimental runs are based on a full factorial design matrix ($2^4 = 16$). The subsequent 8 runs involve combinations of each process variable. The center points are defined with all variables set at the intermediate (0) level, while the star points consist of combinations where each variable is set at either its lowest (-2) or highest (+2) level, with the other three variables held at the intermediate level. The remaining 7 runs have all variables set at the intermediate level (0), representing additional center points. This set of 31 experimental runs allows for the estimation of linear, quadratic, and two-way interactive effects of the process parameters on the responses.

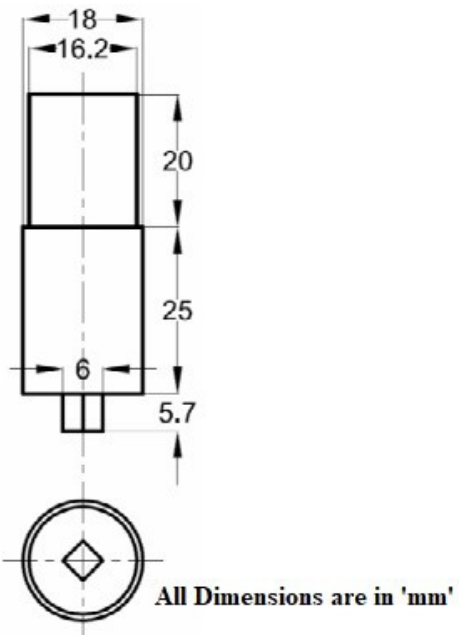

Figure 2. Dimensions of Friction Stir Welding tool.

2.5. Conducting the experiments as per the design matrix

Friction Stir Welding (FSW) employs a non-consumable rotating tool consisting of two parts which include a shoulder and pin. During FSW, the tool pin is inserted into the faying surface of the plates and then moved horizontally in the direction of the weld joint line as shown in Figure 3. The experiments were conducted according to the design matrix (Table 4) using a square butt joint configuration with dimensions of 100 mm × 50 mm × 6 mm (AA6092/ B_4C composite plates), employing a single-pass butt welding procedure. Before Friction Stir Welding, surface oxides were removed from the plates using wire brushing, and the welding direction was aligned with the rolling direction of the plates. To minimize the influence of unknown nuisance variables, thirty-one weld runs were randomly selected from the design matrix. A semi-automatic Friction Stir Welding (FSW) machine (M/s RV Machine Tools, Coimbatore, INDIA) was used, with the tool rotational speed and welding speed adjusted for each test run. The tool pin was plunged into the abutting surfaces until the shoulder made contact, and the specified axial load was applied to maintain pressure during the process. After a short dwell period, which generated sufficient frictional heat to plasticize the material, the FSW machine table advanced at a constant speed as defined in the design matrix. The axial load was kept constant throughout each run, ensuring uniform conditions for all subsequent welding operations. A typical experimental setup of the FSW machine and friction stir welded plate is shown in Figure 3. The wear rate (W), wear resistance (R) and Relative wear rate (WR) were calculated and given in Table 5.

Table 3. Chemical composition of High Carbon High Chromium steel.

Element	C	Mn	Si	Co	Cr	Mo	V	P	Ni	Cu	S
Wt. %	1.4-1.6	0.6	0.6	1	11-13	0.7-1.2	1.1	0.03	0.3	0.25	0.03

Table 4. Process parameters and its levels.

S. No.	Process Parameter	Notation	Unit	Levels				
				-2	-1	0	1	2
1.	Tool Rotational Speed	TRS	rpm	1000	1075	1150	1225	1300
2.	Welding Speed	WS	mm/min	30	40	50	60	70
3.	Axial Load	AL	kN	4	5	6	7	8
4.	% of B_4C	C	Wt.%	0	2.5	5	7.5	10

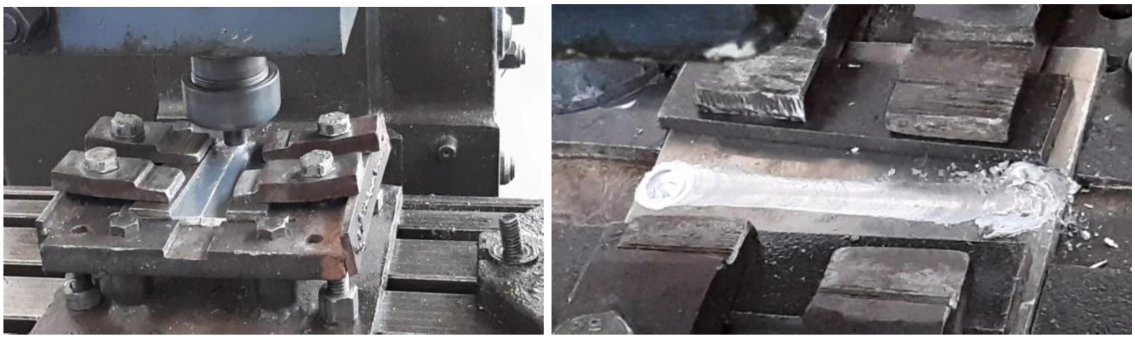

Figure 3. Photograph showing typical FSW experimental set up and friction stir welded plate.

Table 5. Design matrix and experimental results.

Run	Tool Rotational Speed (rpm)	Welding Speed (mm/min)	Axial Load (kN)	% of B_4C (Wt.%)	Wear Rate (1×10^{-5} mm^3/m)	Wear Resistance (m/mm^3)	Relative Wear Rate
R1	1075	40	5	2.5	425	235	0.88
R2	1225	40	5	2.5	406	246	0.84
R3	1075	60	5	2.5	412	243	0.85
R4	1225	60	5	2.5	437	229	0.91
R5	1075	40	7	2.5	405	247	0.84
R6	1225	40	7	2.5	429	233	0.89
R7	1075	60	7	2.5	419	239	0.87
R8	1225	60	7	2.5	432	231	0.90
R9	1075	40	5	7.5	278	360	0.64
R10	1225	40	5	7.5	273	366	0.63
R11	1075	60	5	7.5	279	358	0.65
R12	1225	60	5	7.5	287	348	0.66
R13	1075	40	7	7.5	262	382	0.61
R14	1225	40	7	7.5	284	352	0.66
R15	1075	60	7	7.5	257	389	0.59
R16	1225	60	7	7.5	286	350	0.66
R17	1000	50	6	5	365	274	0.79
R18	1300	50	6	5	397	252	0.86
R19	1150	30	6	5	386	259	0.83
R20	1150	70	6	5	362	276	0.78
R21	1150	50	4	5	364	275	0.79
R22	1150	50	8	5	379	264	0.82
R23	1150	50	6	0	429	233	0.80
R24	1150	50	6	10	170	588	0.38
R25	1150	50	6	5	328	305	0.71
R26	1150	50	6	5	343	292	0.74
R27	1150	50	6	5	323	310	0.70
R28	1150	50	6	5	346	289	0.75
R29	1150	50	6	5	340	294	0.73
R30	1150	50	6	5	316	316	0.68
R31	1150	50	6	5	326	307	0.70

3. Evolving an Empirical Relationships

The response functions representing the wear rate (W) and wear resistance (R) of friction stir welded plates are dependent on tool rotational speed (TRS), welding speed (WS), axial load (AL), and the weight percentage of B_4C (C). These relationships can be expressed[21-23] as:

$$W = f(TRS,\ WS,\ AL,\ C) \tag{5}$$

$$R = f(TRS,\ WS,\ AL,\ C) \tag{6}$$

The second-order polynomial (regression) equation[22,23] employed to denote the response surface is expressed by

$$X = a_0 + \sum a_i x_i + \sum a_{ii} x_i^2 + \sum a_{ij} x_i x_j + \varepsilon \tag{7}$$

A second-order polynomial regression model is used to represent the response surface for the variable 'X'. In this model, a_0 is the average response; a_i, a_{ii} and a_{ij} are coefficients reliant on the major and interaction influences of the parameters; and ε is the statistical error. The coefficients were calculated using Design Expert software and tested for significance at a 95% confidence level. Insignificant terms were removed from the model without sacrificing its accuracy, thereby simplifying the regression process. The finalized regression models for predicting wear rate (W) and wear resistance (R) in friction stir welded joints are presented in coded form, including only the significant control parameters. The final regression equations for calculating W and R in the FSW of AA6092 composites are given in Equations 8 and 9, respectively. Table 6 presents the results of the ANOVA for wear rate (W). To assess the significance of each term in the regression model, a 95% confidence level and a 5% significance level were employed. The analysis revealed that the factors which significantly influence wear rate (W) are Percentage of B_4C (most significant impact), Interaction between Tool Rotational Speed and Axial Load (second-highest influence) and Tool Rotational Speed (third-highest influence) on the wear rate (W). These factors were determined to be significant based on their associated p-values, which were all less than 0.05. Additionally, the lack-of-fit test was conducted to evaluate the adequacy of the developed regression model. The calculated F-value for lack of fit was 1.33, which is substantially lower than the standard F-value of 59.98 at the 95% confidence level. This indicates that the regression model provides an adequate fit to the data and can be reliably used to predict wear rate (W) within the specified range of FSW process parameters and their respective levels.

$$\begin{aligned} W\left(\times 10^{-5}\right),\ mm^3/m &= 4092.8719 - (5.01634 \times TRS) - \\ &(13.2693 \times WS) - (168.0863 \times AL) - (9.2393 \times C) + \\ &(0.0044 \times TRS \times WS) + (0.0658 \times TRS \times AL) + (0.0037 \times TRS \times C) - \\ &(0.1187 \times WS \times AL) - (0.0575 \times WS \times C) - (0.8250 \times AL \times C) + \\ &\left(0.0019 \times TRS^2\right) + \left(0.0919 \times WS^2\right) + \left(8.5610 \times AL^2\right) - \left(1.5102 \times C^2\right) \end{aligned} \tag{8}$$

$$\begin{aligned} WR,\ m/mm^3 &= -3246.5073 + (4.7202 \times TRS) + (12.1811 \times WS) + \\ &(169.5570 \times AL) - (2.9673 \times C) - (0.0037 \times TRS \times WS) - \\ &(0.0698 \times TRS \times AL) - (0.0162 \times TRS \times C) + (0.1519 \times WS \times AL) + \\ &(0.0144 \times WS \times C) + (1.0668 \times AL \times C) - \left(0.0018 \times TRS^2\right) - \\ &\left(0.0888 \times WS^2\right) - \left(8.4676 \times AL^2\right) + \left(4.3003 \times C^2\right) \end{aligned} \tag{9}$$

Table 7 presents the results of the ANOVA for wear resistance (WR). To assess the significance of each term in the regression model, a 95% confidence level and a 5% significance level were employed. The analysis revealed that

Table 6. ANOVA results for Wear Rate (W).

Source	Sum of Squares	df	Mean Square	F-value	p-value	
Model	1.297E+05	14	e9266.24	59.98	< 0.0001	significant
A-Tool Rotational Speed	224.02	1	224.02	1.45	0.2460	
B-Welding Speed	29.17	1	29.17	0.1888	0.6697	
C-Axial Load	50.38	1	50.38	0.3261	0.5759	
D-% of B_4C	19269.14	1	19269.14	124.72	< 0.0001	
AB	175.56	1	175.56	1.14	0.3023	
AC	390.06	1	390.06	2.52	0.1316	
AD	7.56	1	7.56	0.0489	0.8277	
BC	22.56	1	22.56	0.1460	0.7074	
BD	33.06	1	33.06	0.2140	0.6499	
CD	68.06	1	68.06	0.4405	0.5163	
A^2	3419.95	1	3419.95	22.14	0.0002	
B^2	2412.99	1	2412.99	15.62	0.0011	
C^2	2095.81	1	2095.81	13.57	0.0020	
D^2	2547.72	1	2547.72	16.49	0.0009	
Residual	2472.01	16	154.50			
Lack of Fit	1702.58	10	170.26	1.33	0.3786	not significant
Pure Error	769.43	6	128.24			
Cor Total	1.322E+05	30				

Table 7. ANOVA results for Wear Resistance (WR).

Source	Sum of Squares	df	Mean Square	F-value	p-value	
Model	1.550E+05	14	11074.19	35.62	< 0.0001	significant
A-Tool Rotational Speed	487.30	1	487.30	1.57	0.2286	
B-Welding Speed	1.80	1	1.80	0.0058	0.9402	
C-Axial Load	121.65	1	121.65	0.3913	0.5405	
D-% of B_4C	53211.08	1	53211.08	171.15	< 0.0001	
AB	125.06	1	125.06	0.4023	0.5349	
AC	438.27	1	438.27	1.41	0.2524	
AD	147.35	1	147.35	0.4739	0.5010	
BC	36.91	1	36.91	0.1187	0.7349	
BD	2.05	1	2.05	0.0066	0.9363	
CD	113.81	1	113.81	0.3661	0.5536	
A^2	2892.32	1	2892.32	9.30	0.0076	
B^2	2252.88	1	2252.88	7.25	0.0160	
C^2	2050.34	1	2050.34	6.59	0.0206	
D^2	20656.99	1	20656.99	66.44	< 0.0001	
Residual	4974.44	16	310.90			
Lack of Fit	4337.32	10	433.73	4.08	0.0493	significant
Pure Error	637.12	6	106.19			
Cor Total	1.600E+05	30				

the factors like Percentage of B_4C (first greatest contribution), Interaction between Tool Rotational Speed and Axial Load (second-highest influence) and Tool Rotational Speed (third-highest influence) significantly influence wear resistance (WR). These factors were determined to be significant based on their associated p-values, which were all less than 0.05. Additionally, the lack-of-fit test was conducted to evaluate the adequacy of the developed regression model. The calculated F-value for lack of fit was 4.08, which is substantially lower than the standard F-value of 35.62 at the 95% confidence level. This indicates that the regression model provides an adequate fit to the data and can be reliably used to predict wear resistance (WR) within the specified range of FSW process parameters and their respective levels.

4. The Effect of the FSW Process Parameters on the Responses (W and WR)

4.1. Wear Rate (W)

This section analyses the effect of FSW process parameters on three response variables: Wear Rate (W) and Wear Resistance (WR). The interaction effects of two input process parameters on these responses were evaluated, while the third parameter was held constant at its mean value. For W, the perturbation plot (Figure 4) illustrates how the FSW process parameters influence the response within the optimized design framework. The plot shows how W varies as each parameter deviates from its reference value, with all other parameters remaining constant. The results indicate that Tool Rotational Speed (TRS) has the most significant effect on W, followed by Welding Speed (WS) and Axial Load (AL) in decreasing order of influence. Furthermore, the plot highlights that the weight percentage of B_4C (Wt. % B_4C) has the greatest impact on UTS, followed by TRS, AL, and WS.

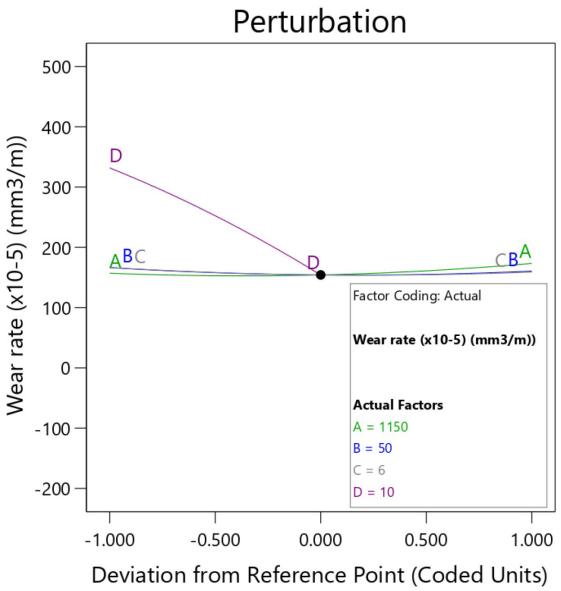

Figure 4. Perturbation plot (impact of process parameters on the W).

The interaction effects of Tool Rotational Speed (TRS), Welding Speed (WS), Axial Load (AL), and B_4C content (W) on Wear Rate (W) are illustrated in Figures 5, 6 and 7. Figures 5a and 5b display the influence of TRS and WS on W, while keeping AL and C constant at 6 kN and 10 wt.%, respectively. The 2D contour plot in Figure 5a shows concentric circles representing tensile strength (in MPa), with the optimal W value located at the centre of the plot. Specifically, the minimum W of 154.67 $x10^{-5}$ mm^3/m is attained at a TRS of 1150 rpm and a WS of 50 mm/min, as shown in both Figures 5a and 5b.

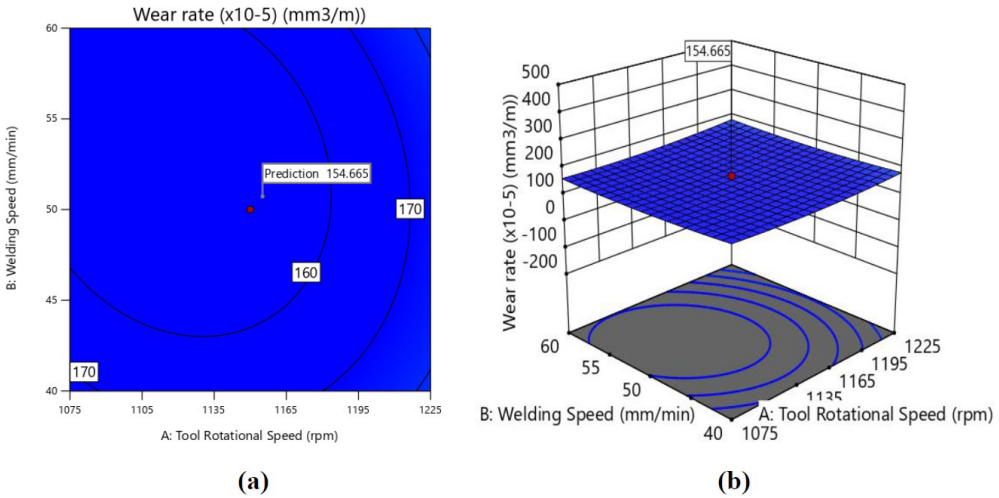

Figure 5. (a) 2D contour plot, (b) 3D contour plot (effect of TRS and WS on W of FSW joint).

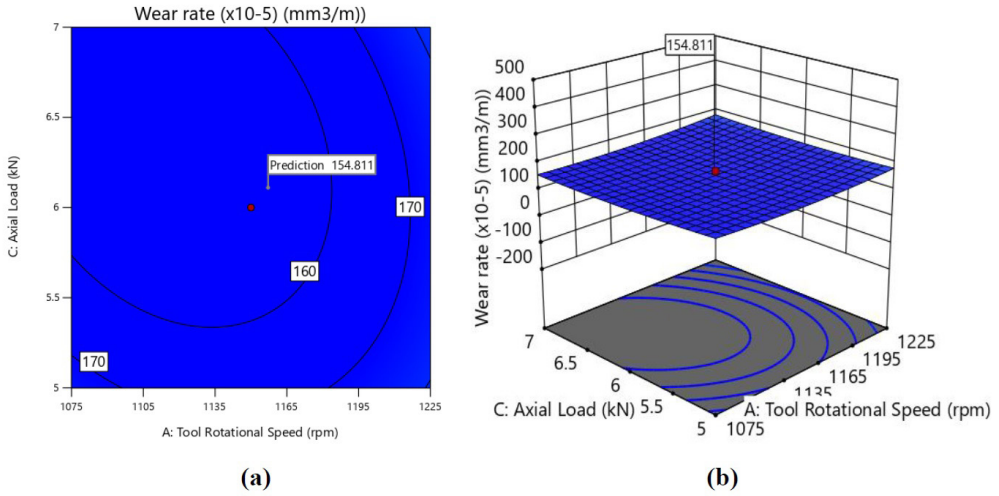

Figure 6. (a) 2D contour plot, (b) 3D contour plot (effect of TRS and AL on W of FSW joint).

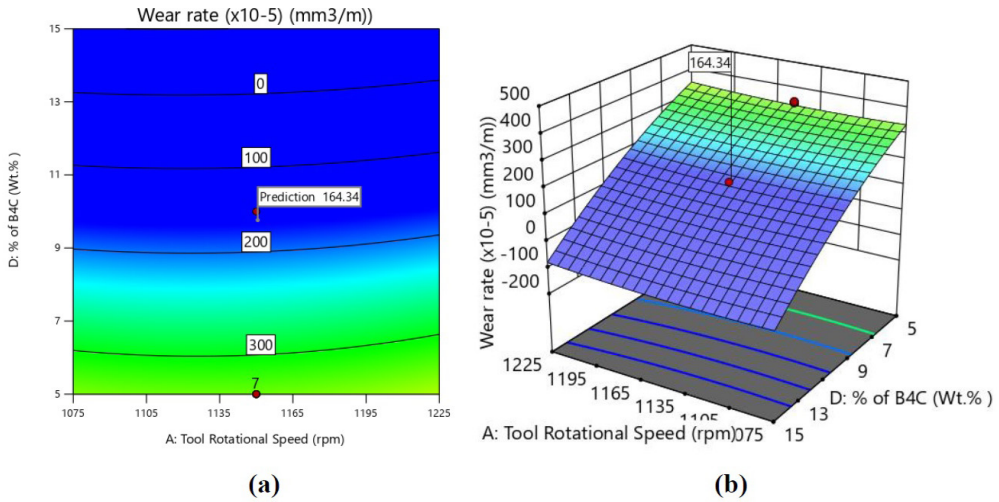

Figure 7. (a) 2D contour plot, (b) 3D contour plot (effect of TRS and C on W of FSW joint).

Figure 6 illustrates the interaction effect of AL and TRS on W, with WS and W held constant at 50 mm/min and 10 wt.%, respectively. The optimal W of approximately 154.67 x10^{-5} mm^3/m is observed at a TRS of 1150 rpm and an AL of 6 kN, as depicted in both the 2D and 3D plots.

Figure 7 illustrates the interaction effect of C and TRS, with AL and WS held constant at 6 kN and 50 mm/min, respectively. The optimal UTS, around 164.34 x10^{-5} mm^3/m (as shown in both 2D and 3D plots), is achieved at a TRS of 1150 rpm and a C of 10 wt.% B_4C.

Similarly, Figure 8 demonstrates the interaction effect of AL and WS, with TRS and C kept constant at 1150 rpm and 10 wt.%. The optimal W, approximately 154.21 x10^{-5} mm^3/m (evident in both 2D and 3D plots), occurs at a WS of 50 mm/min and an AL of 6 kN.

Figure 9 shows the interaction effect of C and WS, with AL and TRS held constant at 6 kN and 1150 rpm, respectively. The optimal W, approximately 154.21 x10^{-5} mm^3/m (as demonstrated in both 2D and 3D plots), is achieved at a WS of 50 mm/min and a C of 10 wt.% B_4C. Similarly, Figure 10 illustrates the interaction effect of C and AL, with TRS and WS kept constant at 1150 rpm and 50 mm/min, respectively. The optimal W, around 154.21 x10^{-5} mm^3/m (as shown in both 2D and 3D plots), is attained at a C of 10 wt.% B_4C and an AL of 6 kN.

4.2. Wear Resistance (WR)

Figure 11 (perturbation plot) illustrates the effect of FSW process parameters on WR for an optimized design. It is evident that across all operational levels of TRS, the

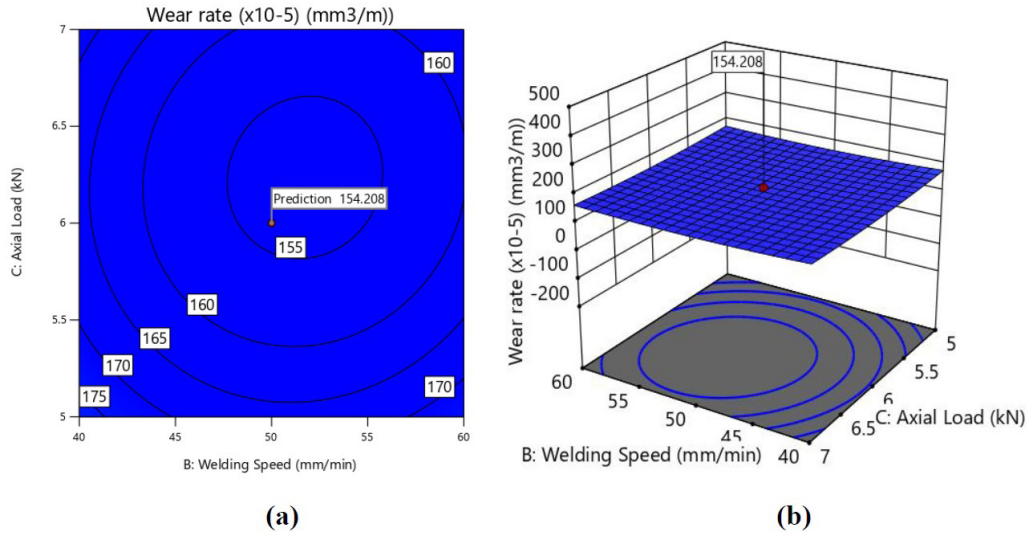

Figure 8. (a) 2D contour plot, (b) 3D contour plot (effect of AL and WS on W of FSW joint).

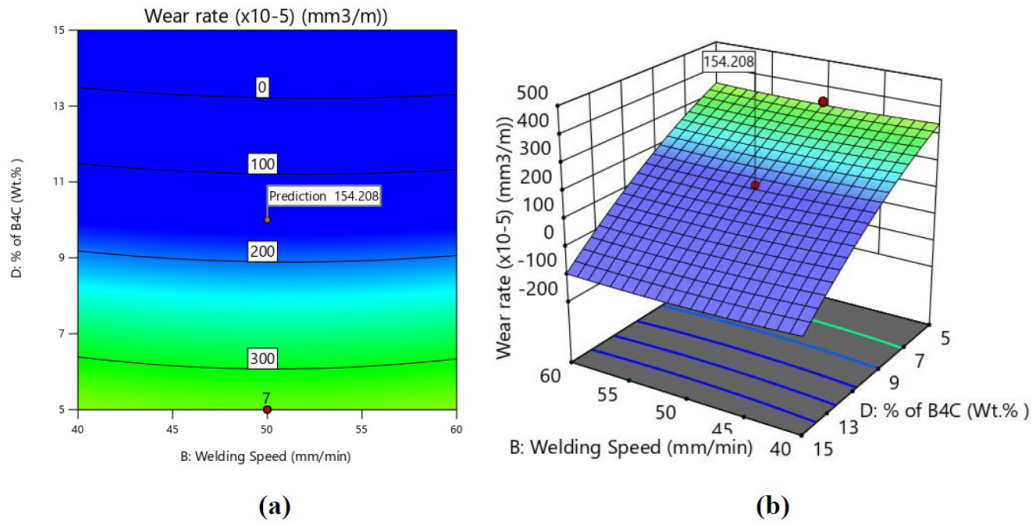

Figure 9. (a) 2D contour plot, (b) 3D contour plot (effect of W and WS on W of FSW joint).

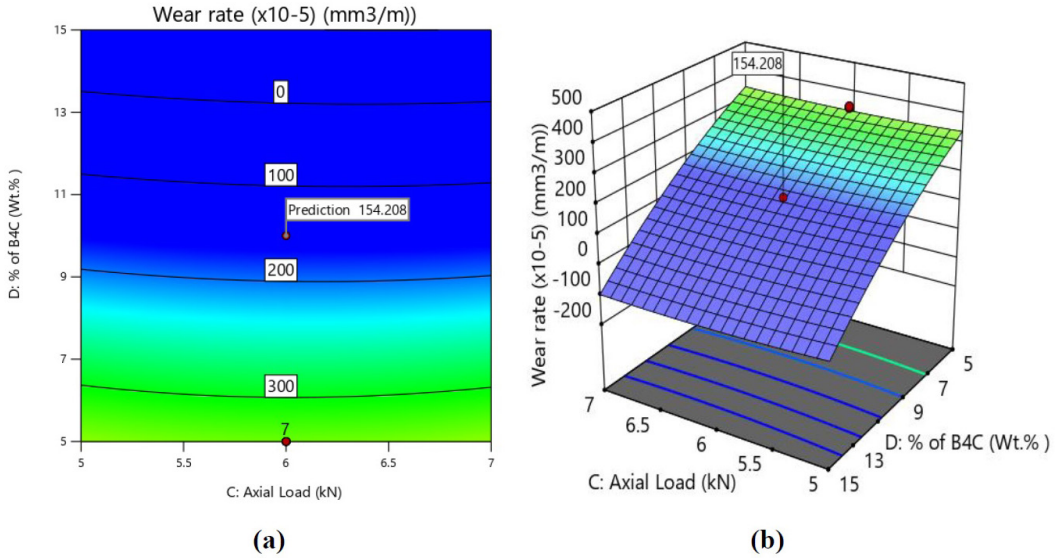

Figure 10. (a) 2D contour plot, (b) 3D contour plot (effect of W and AL on W of FSW joint).

wear resistance consistently betters that of the base metal. The plot also shows that the Wt.% of B_4C has the most significant impact on WR, followed by TRS, AL, and WS.

Figures 12 through 17 depict the interaction effects of Tool Rotation Speed (TRS), Welding Speed (WS), Applied Load (AL), and the Wt.% of B_4C on Wear Resistance (WR). Figures 12a and 12b show the influence of TRS and WS on WR while keeping AL constant at 6 kN. In the 2D contour plot (Figure 12a), concentric circles represent Wear Resistance (m/mm^3), with the optimal value at the centre. The maximum WR of 551.97 m/mm^3 (Figures 12a and 12b) is achieved at a TRS of 1150 rpm and a WS of 50 mm/min.

Figure 13 illustrates the interaction between AL and TRS at a constant WS of 50 mm/min and C of 10 wt.% B_4C. The optimal WR of approximately 551.97 m/mm^3 (as indicated in both 2D and 3D plots) occurs at a TRS of 1150 rpm and an AL of 6 kN. Figure 14 shows the interaction between C and TRS, with WS and AL held constant at 50 mm/min and 6 kN, respectively. The optimal WR of 551.97 m/mm^3 (evident in both 2D and 3D plots) is achieved at a TRS of 1150 rpm and C of 10 wt.% B_4C. Figure 15 demonstrates the effect of WS and AL on WR, with a constant TRS of 1150 rpm and C of 10 wt.% B_4C. The optimal WR, approximately 551.97 m/mm^3 (as shown in the 2D and 3D plots), is achieved at a WS of 50 mm/min and an AL of 6 kN.

Figure 16 highlights the influence of C and WS on WR under constant TRS of 1150 rpm and AL of 6 kN. The optimal WR, around 551.97 m/mm^3 (visible in the 2D and 3D plots), occurs at a WS of 50 mm/min and C of 10 wt.% B_4C. Lastly, Figure 17 emphasizes the effect of C and AL on WR, with TRS and WS kept constant at 1150 rpm and 50 mm/min, respectively. The optimal WR, approximately 551.97 m/mm^3 (as seen in the 2D and 3D plots), is attained at an AL of 6 kN and a C of 10 wt.% B_4C.

5. Results of Optimization

Following the optimization study aimed at achieving the desired tribological properties for the welded joint,

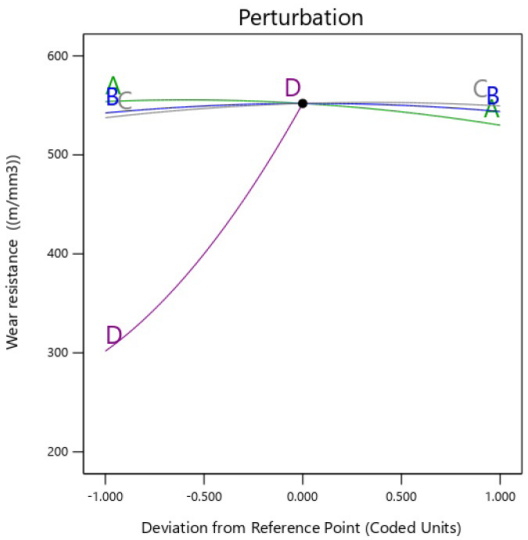

Figure 11. Perturbation plot (effect of process parameters on the WR).

the optimal welding conditions were selected based on the criteria outlined in Table 8. The experimental and optimization results indicate that a Tool Rotational Speed (TRS) of approximately 1150 rpm is ideal for optimizing Wear Rate (W), and Wear Resistance (WR). Among the input parameters, the Wt.% of B_4C has the most significant influence on these responses. The optimized FSW process parameters and the responses predicted by the design expert software are summarized in Table 9.

5.1. Validation of the developed model

The empirical or mathematical model developed using the desirability approach was validated by comparing its predictions with experimental results, with errors calculated for all thirty-one runs (Table 5). The experimental values

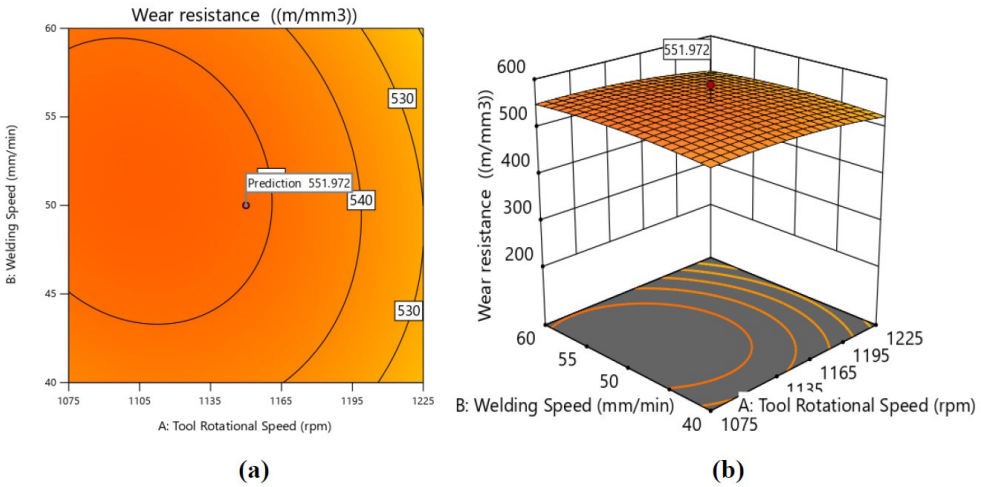

Figure 12. (a) 2D contour plot, (b) 3D contour plot (effect of TRS and WS on WR of FSW joint).

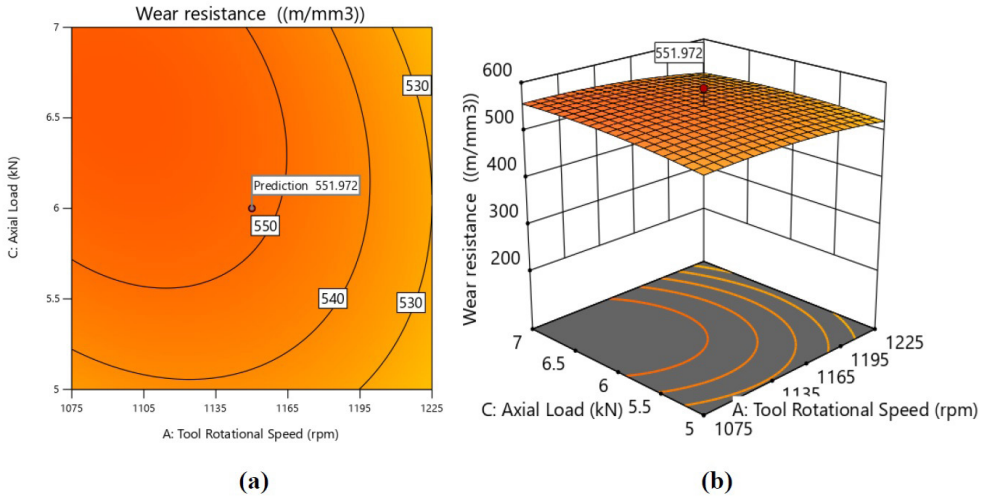

Figure 13. (a) 2D contour plot, (b) 3D contour plot (effect of TRS and AL on WR of FSW joint).

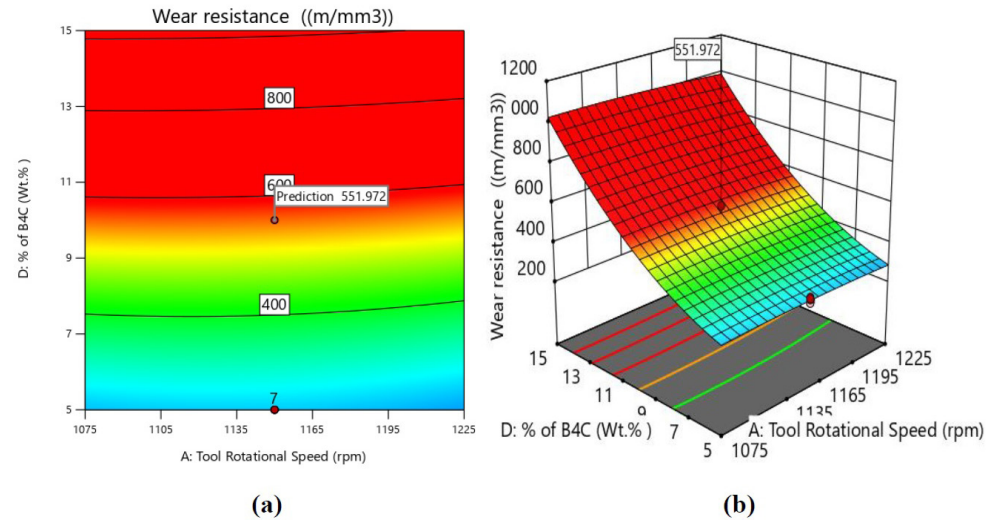

Figure 14. (a) 2D contour plot, (b) 3D contour plot (effect of C and TRS on WR of FSW joint).

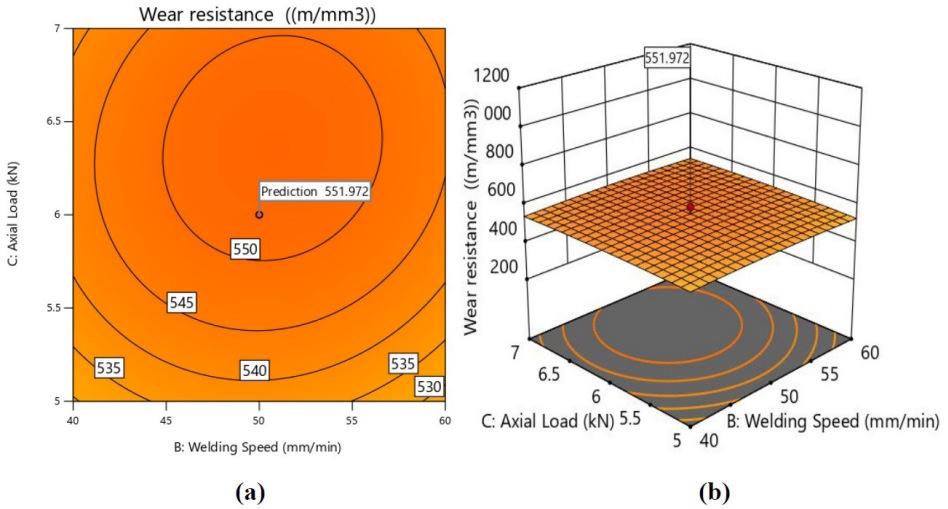

Figure 15. (a) 2D contour plot, (b) 3D contour plot (effect of AL and WS on WR of FSW joint).

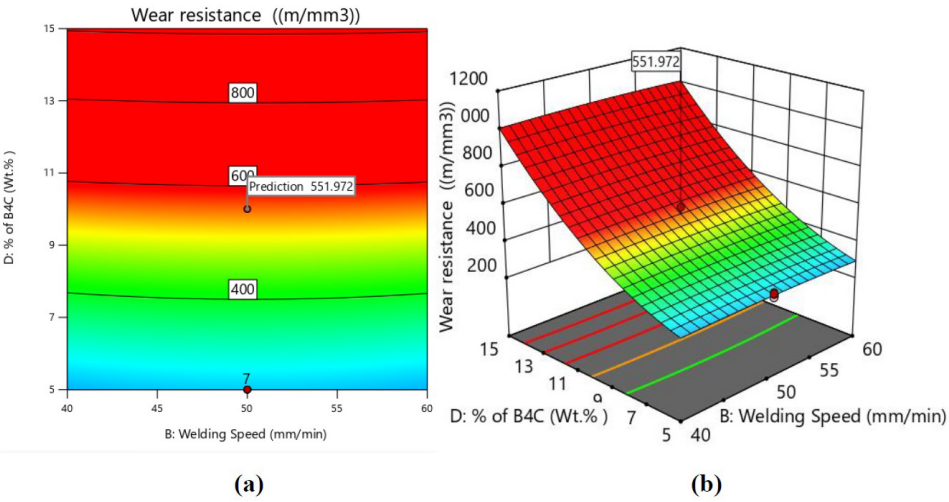

Figure 16. (a) 2D contour plot, (b) 3D contour plot (effect of C and WS on WR of FSW joint).

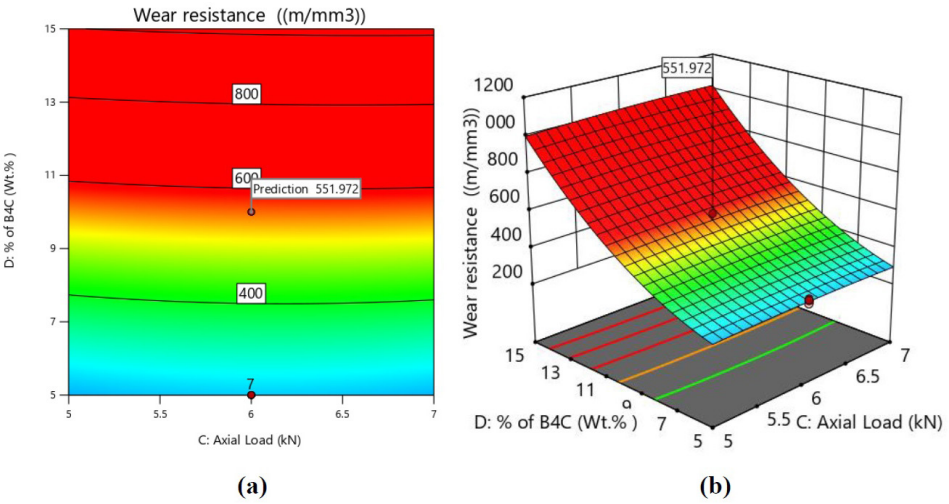

Figure 17. (a) 2D contour plot, (b) 3D contour plot (effect of C and AL on WR of FSW joint).

Table 8. Optimization criteria used in this work.

Process Parameters / Responses	Goal	Minimum Limit	Maximum Limit	Importance
Tool Rotational Speed	is in range	1075	1225	3
Welding Speed	is in range	40	60	3
Axial Load	is in range	5	7	3
Wt.% B_4C	is in range	5	15	3
Wear Rate (1 x10^{-5})	minimize	437	170	5
Wear Resistance	maximize	229	588	5

Table 9. Optimized FSW process parameters and responses predicted by design expert. software.

Tool rotational speed (rpm)	Welding Speed (mm/min)	Axial load (kN)	Wt.% of B_4C	Wear Rate (1 x10^{-5} mm^3/m)	Wear Resistance (m/mm^3)
1150	50	6	10	154.21	551.97

Table 10. Experimental and predicted values for thirty-one runs.

Run	Wear Rate (1 x10^{-5} mm^3/m)			Wear Resistance (m/mm^3)		
	Experimental Value	Predicted Value	Error in %	Experimental Value	Predicted Value	Error in %
R1	425	418	1.65	235	230	2.13
R2	406	413	-1.72	246	240	2.44
R3	412	419	-1.70	243	249	-2.47
R4	437	429	1.83	229	235	-2.62
R5	405	415	-2.47	247	255	-3.24
R6	429	437	-1.86	233	239	-2.58
R7	419	426	-1.67	239	234	2.09
R8	432	426	1.39	231	225	2.60
R9	278	284	-2.16	360	369	-2.50
R10	273	285	-4.40	366	372	-1.64
R11	279	286	-2.51	358	350	2.23
R12	287	283	1.39	348	356	-2.30
R13	262	275	-4.96	382	378	1.05
R14	284	289	-1.76	352	360	-2.27
R15	257	267	-3.89	389	380	2.31
R16	286	293	-2.45	350	356	-1.71
R17	365	373	-2.19	274	282	-2.92
R18	397	405	-2.02	252	260	-3.17
R19	386	393	-1.81	259	265	-2.32
R20	362	369	-1.93	276	284	-2.90
R21	364	373	-2.47	275	269	2.18
R22	379	386	-1.85	264	257	2.65
R23	429	436	-1.63	233	239	-2.58
R24	170	174	-2.16	588	572	2.72
R25	328	335	-2.13	305	313	-2.62
R26	343	349	-1.75	292	296	-1.37
R27	323	330	-2.17	310	317	-2.26
R28	346	352	-1.73	289	294	-1.73
R29	340	351	-3.24	294	286	2.72
R30	316	324	-2.53	316	322	-1.90
R31	326	318	2.45	307	317	-3.26

were obtained through actual testing, while the predicted values were derived from the empirical equations generated by the design expert software. Table 10 presents the experimental values, predicted values, and percentage errors for Wear Rate (W) and Wear Resistance (WR). For W, the percentage error ranges from - 4.96% to + 1.39%, and for WR from - 3.24% to + 1.05%. These results indicate that the developed model accurately predicts W, and WR, as the predicted values closely align with the experimental outcomes.

The results of the validation experiments are summarized in Table 11. To evaluate the model's accuracy under the predicted optimal welding conditions, three confirmation experiments were conducted. These experiments used a Tool Rotation Speed (TRS) of 1150 rpm, a Welding Speed (WS) of 50 mm/min, and an Applied Load (AL) of 6 kN. The maximum percentage errors observed between the predicted and experimental results for Wear Rate (W), and Wear Resistance (WR) were +5.39%, and +2.65%, respectively.

6. Analysis of Worn Surface

The SEM micrograph of the typical base metal composite is shown in Figure 18a, revealing strong bonding between the reinforcement and the matrix. After the FSW process, substantial grain refinement in the matrix and a reduction in B_4C particle size are observed in the stir zone, as shown in Figure 18b. During the FSW process, the stir zone undergoes severe plastic deformation, with material flow driven by the stirring action of the tool pin. The frictional heat generated by the rotating tool, combined with stress-induced plastic deformation in the weld zone, stretches the B_4C particles along the shear stress directions. The weld nugget zone exhibits a recrystallized microstructure, with a higher concentration of B_4C particles dispersed in the matrix.

In the FSW of composites, grain refinement is further enhanced by the reinforcing material, as the particles provide additional nucleation sites that facilitate grain growth. The inverse relationship between the number of nucleation sites and grain size can be exploited in aluminum metal matrix composites (AMMCs) to reduce grain size in the finished joint. The stirring action of the tool pin abrades the surface of the B_4C particles into smaller fragments, as evident in Figure 18b. The presence of these fine particles, combined with a refined grain matrix, significantly enhances the strength of the composite in the stir zone.

Figures 19a-d show SEM micrographs of the abraded worn surface of FSW AMMCs containing 2.5%, 5%, 7.5%, and 10% B_4C by weight, respectively. Various wear mechanisms, such as grooves, localized plastic deformation, and tearing, were observed. The significant plastic deformation in the aluminum matrix leads to particle fracture and particle transfer between interfaces during wear. Figure 19a depicts the worn surface of the composite with 2.5% B_4C, revealing deep grooves, numerous pits, and cracks. It was reported that deformation in the matrix is minimal at lower loads, but increases considerably under higher loads. In the initial stages of wear, the cutting and ploughing mechanism involves fragmentation of asperities and material removal due to the cutting action of hard asperities against the softer pin surface[24].

As sliding distance increases, frictional heat accumulates, causing the temperature at the contact surface to rise monotonically due to adiabatic heating. This elevated temperature softens the pin surface, increasing the rate of deformation. Subsurface microcracks form and eventually lead to the removal of wear debris, resulting in the formation of transverse and longitudinal wear tracks. At the initial stage of sliding wear, the aluminum matrix surrounding the particles is worn away, exposing the reinforcing particles, which come into contact with the steel counter face. Once exposed, the wear rate decreases as these harder particles resist further wear.

During the wear test, sliding exerts significant tangential force on the particles in contact with the counter face

Table 11. Validation of test results.

Run	Tool Rotational Speed (rpm)	Welding Speed (mm/min)	Axial Load (kN)	Wt.% of B_4C	W (1 x10^{-5} mm^3/m)			WR (m/mm^3)		
					Actual value	Predicted value	Error in %	Actual value	Predicted value	Error in %
R1	1150	50	6	10	162	154.21	4.81	566	551.97	2.47
R2	1150	50	6	10	160	154.21	3.62	567	551.97	2.65
R3	1150	50	6	10	163	154.21	5.39	565	551.97	2.31

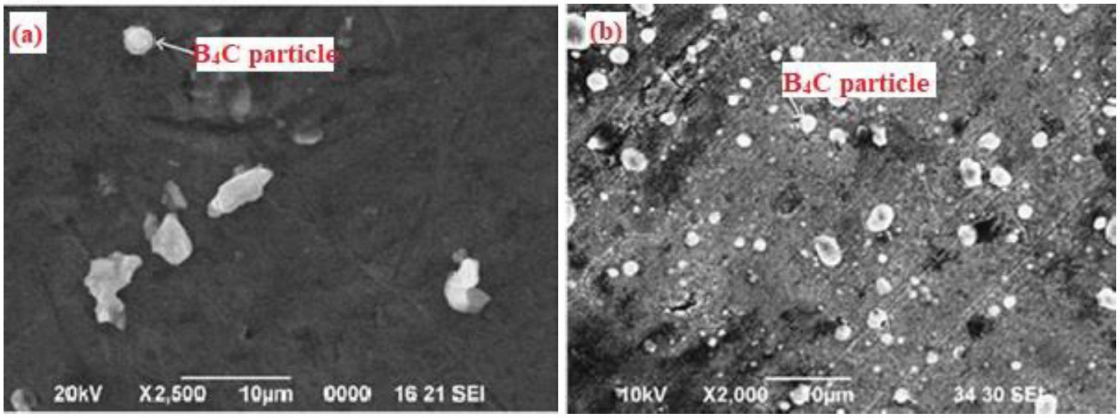

Figure 18. SEM images of AA6092 -10% B_4C composite: (a) before FSW process and (b) after FSW process.

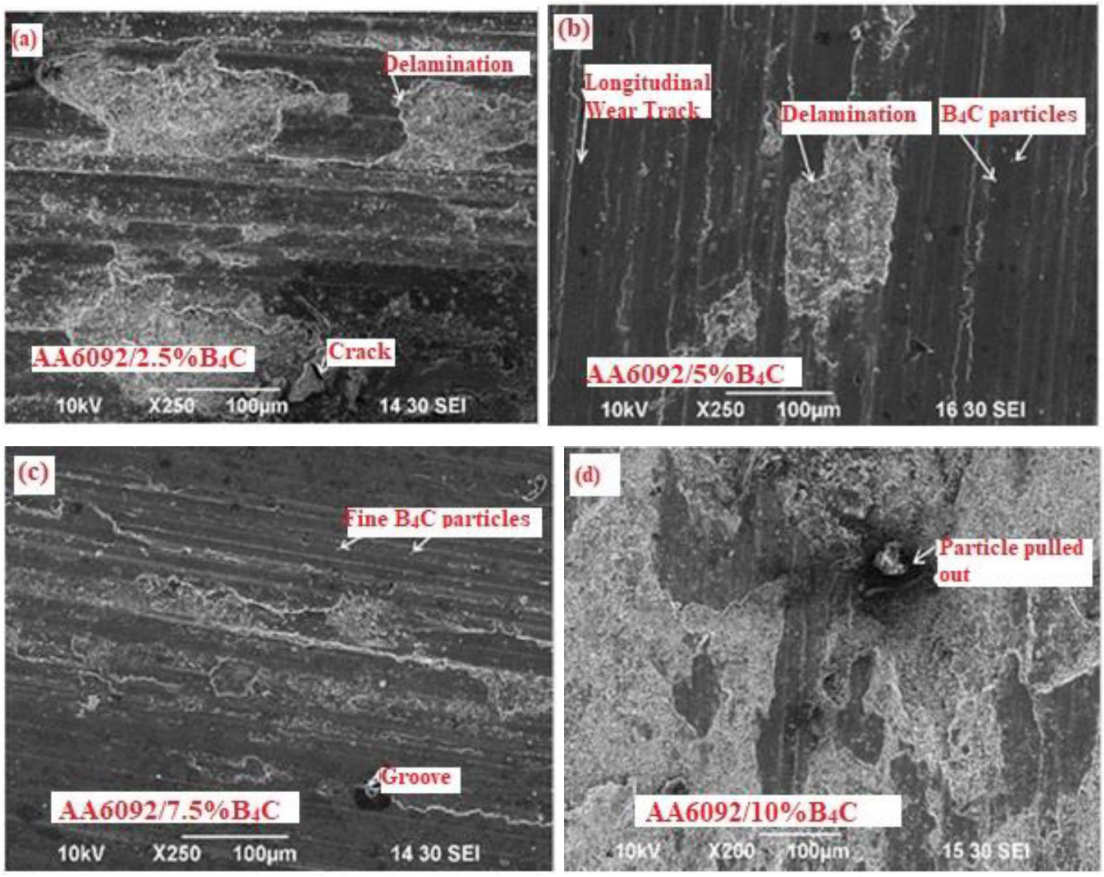

Figure 19. SEM images of worn surface of the FSW AA6092-B_4C composite containing: (a) 2.5% B_4C; (b) 5% B_4C; (c) 7.5% B_4C; and (d) 10% B_4C.

material, generating localized shear stress that can cause particle fracture or pull-out. The shear stress also promotes dislocation slip, leading to delamination of the hardened layer from the pin specimen. Finer particles embedded in the matrix are observed in Figures 19b and 19c, where the wear debris is round and makes increased contact with the counter face. Additionally, finer grooves are visible on the worn surface of the matrix. The wear rate decreases due to finer grain refinement in the matrix and the increased hardness of the composite. Figures 19d shows less plastic deformation and finer grooves for the composites containing 10% B_4C, respectively. Overall, the wear rate of the composite decreases as the content of reinforcing particles increases[25].

6.1. Effect of tool rotational speed on wear rate

An observable decrease in wear rate occurs as tool rotational speed increases from 1000 rpm to 1150 rpm. During the FSW process, higher rotational speeds result in increased heat input to the weld zone, leading to sufficient plastic deformation. This rise in speed also abrades the B_4C particles, allowing for better dispersion within the weld zone. The enhanced distribution of particles in the stir zone contributes to a reduced wear rate. Additionally, these particles may fragment into finer particles that spread across the wear surface, providing further protection to the matrix against severe wear. However, as the tool rotational speed increases from 1150 rpm to 1300 rpm, the wear rate begins to rise again. This increase may be attributed to excessive heat input, which can lead to the debonding of B_4C particles from the matrix.

6.2. Effect of welding speed on wear rate

The wear rate of the AA6092/B_4C composite decreases as the welding speed increases from 30 mm/min to 50 mm/min. At lower traverse speeds, specifically between 30 mm/min and 50 mm/min, a uniform equiaxed grain structure with consistent dispersion of B_4C particles in the matrix is formed, which enhances the material's strength. This improved strength significantly contributes to wear resistance. However, when the tool traverse speed exceeds 50 mm/min (up to 70 mm/min), the heat input to the material diminishes. This results in inadequate plastic behavior, leading to increased delamination and fracture of particles from the matrix, ultimately causing an increase in the wear rate.

6.3. Effect of axial force on wear rate

The data indicate that as the axial force increases from 4 kN to 6 kN, the wear rate decreases to a minimum before rising again with further increases in axial force. The lowest wear rate is observed at an axial force of

6 kN. At this load, the weld joint exhibits uniform grain structure and homogeneous dispersion of B_4C particles in the matrix; however, during wear testing, the surface deformation behavior of the matrix is found to be poor. At higher axial forces, the plunge depth of the tool into the workpiece increases significantly, which reduces the material's strength and results in a higher wear rate.

6.4. Effect of reinforcement on wear rate

The wear rate decreases as the wt.% of B_4C content in the aluminum matrix composites (AMMCs) increases. This reduction is attributed to the higher concentration of particles, which diminishes the matrix grain boundaries, resulting in increased brittleness and higher hardness of the composites[26]. The processing of the Al–B_4C composite with the addition of titanium produces a reaction layer at the matrix-reinforcement interface, acting as a barrier that limits interfacial reactions between B_4C and the aluminum matrix, thereby enhancing interfacial bonding. Increasing the wt.% of B_4C in the matrix reduces ductility while increasing strength. The combination of higher hardness and strong interfacial bonding in the Al/B_4C composites leads to a lower wear rate. Additionally, the average thermal expansion coefficient of AA6092 is 13×10^{-6} /°C, while that of B_4C is 5×10^{-6} /°C. This discrepancy in thermal expansion creates a high density of dislocations around the B_4C particles during solidification. The interaction between these dislocations and B_4C particles further enhances wear resistance. A lower wear rate is observed at a 10% wt. concentration of B_4C in the composite. During the wear test, the higher amount of B_4C particles in the AA6092/10% B_4C aluminum matrix composites (AMMCs) results in more contact between the aluminum matrix and the steel counter face. Consequently, the mass of wear debris generated is lower than that in AMMCs containing more than 10% B_4C. It is widely reported that the incorporation of hard ceramic particles into monolithic alloys significantly enhances the wear resistance of aluminum[27,28].

7. Conclusions

The following conclusions are drawn from this study:

- Empirical models incorporating the welding parameters have been developed to predict the sliding wear behavior of AA6092/0–10 wt.% B_4C composite butt-welded joints.
- The process parameters independently affect the sliding wear behavior across the full range of parameters studied.
- Joints fabricated with a Tool Rotational Speed (TRS) of 1150 rpm, Welding Speed (WS) of 50 mm/min, Axial Load (AL) of 6 kN, and 10 wt.% B_4C exhibit the highest wear resistance.
- Friction Stir Welding (FSW) enhances the wear resistance of the developed aluminum metal matrix composites (AMMCs).
- A shift in wear mode from adhesive wear to abrasive wear is observed as the weight percentage of B_4C particles increases.
- The maximum percentage errors for predicting optimal Wear Rate, and Wear Resistance (WR) were + 5.39%, and + 2.65%, respectively.

8. References

1. Patel M, Sahu SK, Singh MK, Kumar A. Sliding wear behavior of particulate reinforced aluminium metal matrix composites. Int J Eng Res Curr Trends,. 2020;2(3):8-13.
2. Samal P, Mandava RK, Vundavilli PR. Dry sliding wear behavior of Al 6082 metal matrix composites reinforced with red mud particles. SN Applied Sciences. 2020;2(2):313. http://doi.org/10.1007/s42452-020-2136-2.
3. Raju K, Balakrishnan M. Dry sliding wear behavior of aluminum metal matrix composite reinforced with lithium and silicon nitride. Silicon. 2022;14(1):115-25. http://doi.org/10.1007/s12633-020-00793-8.
4. Ramesh CS, Khan S, Khan ZA. Dry sliding-friction and wear behavior of hot-extruded Al6061/Si_3N_4/Cf hybrid metal matrix composite. J Mater Eng Perform. 2020;29(7):4474-83. http://doi.org/10.1007/s11665-020-04940-5.
5. Ashok Kumar B, Murugan N. Optimization of Friction Stir Welding process parameters to maximize tensile strength of stir cast AA6061-T6/AlN_p composite. Mater Des. 2014;57:383-93. http://doi.org/10.1016/j.matdes.2013.12.065.
6. Umar Mohamed J, Palaniappan PLK, Maran P, Pandiyarajan R. Influences of ZrO_2 and B_4C reinforcement on metallurgical, mechanical, and tribological properties of AA6082 hybrid composite materials. J Ceram Process Res. 2021;22:306-16. http://doi.org/10.36410/jcpr.2021.22.3.306.
7. Dinaharan I, Murugan N. Influence of friction stir welding parameters on sliding wear behavior of AA6061/0-10 wt.% ZrB_2 in-situ composite butt joints. J Miner Mater Charact Eng. 2011;10(14):1359-77. http://doi.org/10.4236/jmmce.2011.1014107.
8. Dinaharan I, Murugan N. Effect of friction stir welding on microstructure, mechanical and wear properties of AA6061/ZrB_2 in situ cast composites. Mater Sci Eng A. 2012;543:257-66. http://doi.org/10.1016/j.msea.2012.02.085.
9. Hassan AM, Qasim T, Ghaithan A. Effect of pin profile on friction stir welded aluminum matrix composites. Mater Manuf Process. 2012;27(12):1397-401. http://doi.org/10.1080/10426914.2012.663238.
10. Kalaiselvan K, Murugan N. Dry sliding wear behaviour of Friction Stir Welded aluminum (6061)-B_4C composite. Int. J. Microstructure and Materials Properties. 2013;8(3):239-51. http://doi.org/10.1504/IJMMP.2013.055386.
11. Krishnamurthy K, Ashebre M, Venkatesh J, Suresha B. Dry sliding wear behavior of aluminum 6063 composites reinforced with TiB_2 particles. J Miner Mater Charact Eng. 2017;5(2):74-89. http://doi.org/10.4236/jmmce.2017.52007.
12. Khare M, Gupta RK, Bhardwaj B. Dry sliding wear behaviour of Al 7075/Al_2O_3/B_4C composites using mathematical modelling and statistical analysis. Mater Res Express. 2019;6(12):126512. http://doi.org/10.1088/2053-1591/ab546a.
13. Hillary JJM, Ramamoorthi R, Chelladurai SJS. Dry sliding wear behaviour of Al6061–5%SiC: TiB_2 hybrid metal matrix composites synthesized by stir casting process. Mater Res Express. 2020;7(12):126519. http://doi.org/10.1088/2053-1591/abd19b.
14. Suresh R, Joshi Ajith G, Siddeshkumar NG. Investigation on dry sliding wear behavior of AA5083/nano-Al_2O_3 metal matrix composites. Rev Metal. 2022;58:e213. http://doi.org/10.3989/revmetalm.213.
15. Vijayakumar S, Anitha S, Arivazhagan R, Hailu AD, Rao TVJ, Pydi HP. Wear investigation of aluminum alloy surface layers fabricated through friction stir welding method. Adv Mater Sci Eng. 2022;2022:1-8. http://doi.org/10.1155/2022/4120145.
16. Palanivel R, Koshy Mathews P, Murugan N. Optimization of process parameters to maximize ultimate tensile strength of friction stir welded dissimilar aluminum alloys using response

surface methodology. J Cent South Univ. 2013;20(11):2929-38. http://doi.org/10.1007/s11771-013-1815-1.

17. Pandiyarajan RP, Maran N, Murugan N, Marimuthu S, Sornakumar T. Friction stir welding of hybrid AA 6061-ZrO_2-C composites FSW process optimization using desirability approach. Mater Res Express. 2019;6(6):066553. http://doi.org/10.1088/2053-1591/ab084e.
18. Umar MJ, Palaniappan PLK, Maran P, Pandiyarajan R. Investigation and optimization of Friction Stir Welding process parameters of stir cast AA6082/ ZrO_2 / B_4C composites. Mater Sci Pol. 2020;38(4):715-30. http://doi.org/10.2478/msp-2020-0082.
19. Rajakumar S, Muralidharan C, Balasubramanian V. Optimization of the friction-stir-welding process and tool parameters to attain a maximum tensile strength of AA7075-T6 aluminum alloy. Proc Inst Mech Eng, B J Eng Manuf. 2010;224(8):1175-91. http://doi.org/10.1243/09544054JEM1802.
20. Alidokht SA, Abdollah-Zadeh A, Assadi H. Effect of applied load on the dry sliding wear behaviour and the subsurface deformation on hybrid metal matrix composite. Wear. 2013;305(1-2):291. http://doi.org/10.1016/j.wear.2012.11.043.
21. Rejil CM, Dinaharan I, Vijay SJ, Murugan N. Microstructure and sliding wear behavior of AA6360/(TiC+B_4C) hybrid surface composite layer synthesized by friction stir processing on aluminum substrate. Mater Sci Eng A. 2012;552:336-44. http://doi.org/10.1016/j.msea.2012.05.049.
22. Hemanth J. Tribological behavior of cryogenically treated B_4Cp/Al–12% Si composites. Wear. 2005;258(11-12):1732-44. http://doi.org/10.1016/j.wear.2004.12.009.
23. Mindivan H. Reciprocal sliding wear behavior of B_4C particulate reinforced aluminum alloy composites. Mater Lett. 2010;64(3):405-7. http://doi.org/10.1016/j.matlet.2009.11.032.
24. Naveen Kumar G, Narayanasamy R, Natarajan S, Kumaresh Babu SP, Sivaprasad K, Sivasankaran S. Dry sliding wear behavior of AA 6351-ZrB_2 in situ composite at room temperature. Mater Des. 2010;31(3):1526-32. http://doi.org/10.1016/j.matdes.2009.09.017.
25. Mandal A, Chakraborty M, Murty BS. Effect of TiB_2 particles on sliding wear behavior of Al-4Cu alloy. Wear. 2007;262(1-2):160-6. http://doi.org/10.1016/j.wear.2006.04.003.
26. Akbari M, Asadi P, Aliha MRM, Berto F. Modeling and optimization of process parameters of the piston alloy-based composite produced by FSP using response surface methodology. Surf Rev Lett. 2023;30(6):2350041. http://doi.org/10.1142/S0218625X23500415.
27. Akbari M, Aliha MRM, Berto F. Investigating the role of different components of friction stir welding tools on the generated heat and strain. Forces Mech. 2023;10:100166. http://doi.org/10.1016/j.finmec.2023.100166.
28. Akbari M, Asiabaraki HR. Modeling and optimization of tool parameters in friction stir lap joining of aluminum using RSM and NSGA II. Weld Int. 2023;37(1):21-33. http://doi.org/10.1080/09507116.2022.2164530.